REPORT

A cause and protective treatment for acute and progressive disability and grey matter atrophy

Erika A. Aguzzi,[1,†] Roshni A. Desai,[1,†] Zhiyuan Yang,[1,†] Andrew L. Davies,[1] Don Mahad,[2] Bernard Siow,[3] Ayse G. Yenicelik,[1] Radha Desai,[1] Eleni Giama,[1] AlBeshr Almasri,[1] Miranda Colman,[1] Celine Geywitz,[4] Lucas Schirmer,[4,5,6] Paul A Felts,[7] and Kenneth J. Smith[1]

[†]These authors contributed equally to this work.

Abstract

Acutely inflamed CNS lesions can be sufficiently hypoxic to cause temporary neurological disability. A new experimental lesion reveals that brief hypoxia can also ignite a slow-burning atrophy of the grey matter, resulting in a lifetime of slowly progressive disability. The progressive disability eventually exceeds that observed acutely, indicating that acutely functioning tissue can nevertheless be destined to atrophy. Remarkably, both the temporary initial disability and the ensuing progressive disability and atrophy are significantly reduced if the acute hypoxia is avoided by four days of treatment with vasodilating nimodipine, or by simply breathing raised oxygen concentration. Thus, a lifetime of progressive disability and neurodegeneration can be the legacy of a few days of inflammatory hypoxia experienced in young adulthood, and avoided by maintaining lesion oxygenation. The findings may help to understand and treat some progressive neurological disorders, including multiple sclerosis.

Author affiliations:

1 Department of Neuroinflammation, UCL Queen Square Institute of Neurology, Queen Square, London, WC1N 3BG, UK

2 Centre for Clinical Brain Sciences, University of Edinburgh, Edinburgh, EH16 4SB, UK

3 In Vivo Imaging, Biological Research Facility, The Francis Crick Institute, London, NW1 1AT, UK

4 Division of Neuroimmunology, Department of Neurology, Medical Faculty Mannheim, Heidelberg University, 68167 Mannheim, Germany

5 Mannheim Center for Translational Neuroscience, Heidelberg University, 68167 Mannheim, Germany

6 Interdisciplinary Center for Neurosciences, Heidelberg University, 69120 Heidelberg, Germany

7 Centre for Anatomy and Human Identification, University of Dundee, Nethergate, Dundee, DD1 4HN, Scotland, UK

Correspondence to: Dr Erika A. Aguzzi

UCL Institute of Ophthalmology, 11-43 Bath Street, London, EC1V 9EL, UK

E-mail Erika.aguzzi@ucl.ac.uk

Running title:

Protection from progressive atrophy

Keywords: neuroinflammation; neurodegeneration; grey matter atrophy; neuroprotection; disease progression; relapse

Introduction

Slowly progressive ('smouldering') neurodegeneration and atrophy characterise several neurological disorders, including progressive multiple sclerosis (MS) and Alzheimer's disease[1], but the mechanisms responsible are not understood. A key outstanding question is whether the progressive degeneration in later life is due to contemporaneous events in later life, or whether it can be the delayed expression of damage incurred much earlier. For example, various features of innate neuroinflammation (whether or not provoked by autoimmunity) have been implicated in chronic ongoing neurodegeneration in MS. These include microglial activation, blood brain barrier (BBB) breakdown, actual and virtual tissue hypoxia, mitochondrial impairment especially of respiratory complex IV, and the production of nitric oxide and reactive oxygen species (ROS)[2-6]. However, it remains uncertain whether brief acute exposure to these same factors earlier in life may also result in neurodegeneration but after a substantial delay. It is correspondingly unclear whether acutely targeting any of these factors

in early life may provide a route to achieve protection from later progressive neurodegeneration and disability.

Research has been hindered by a paucity of experimental animal models in which to study the mechanisms and test potential therapies, but here we introduce a model of slowly progressive disability, neurodegeneration and atrophy, and use it to identify a strategy to achieve significant lifetime protection from disability and pathology. The lesion is induced in the grey matter of the spinal cord because many studies have shown that, in MS at least, it is atrophy of the grey matter that is pivotal in determining disability[7], and such atrophy in the spinal cord, rather than brain, has greater association with advancing disability[8].

To explore mechanisms potentially responsible for the slowly progressive disability, and whether targeting the mechanisms may provide a neuroprotective treatment, we considered particular features of the acute lesion. The acutely inflamed lesion labels strongly for markers of hypoxia, which have been shown in other models[9-12] to cause acute and reversible neurological deficits, and to be reversed by treatment with the vasodilating agent nimodipine or by breathing raised oxygen[9,11,12]. We have therefore examined whether these agents may not only reduce the acute disability in the new lesion, but also protect from the progressive accumulation of permanent disability.

Materials and methods

Lesion Induction and Assessment of Neurological Deficit

Young adult male Sprague Dawley rats were anaesthetised (isoflurane; 1.5-2% in room air) and an intraspinal microinjection of the proinflammatory agent lipopolysaccharide (LPS; 0.5 µl of 80 ng/µl in saline) performed into the right ventral horn at the T13 vertebra using methods similar to those previously described[13]. Control animals received similar injections of saline alone. The wound was closed and anaesthesia discontinued. Neurological function was assessed by analysis of gait and tail elevation using video recordings of animals walking freely on a level surface both before lesion induction, and at various times afterwards until termination 6 or 12 months later.

Treatment

Treatments were selected based on observations from the acutely inflamed lesion, which was profoundly hypoxic. Based on our previous observations in other neuroinflammatory and hypoxic lesions[9-12], animals were randomised into groups prior to lesion induction, and treated for just the first four days with either the CNS-selective vasodilating agent nimodipine or inspiratory normobaric oxygen (80%). Both these treatments promptly improve the oxygenation of inflamed CNS tissue[9].

For nimodipine, animals received an intraperitoneal injection while under the surgical anaesthesia (30mg/kg) and then seven additional doses (30mg/kg) by twice daily oral gavage. Animals treated with oxygen (50% or 80% as noted) were placed after anaesthesia in an environment of raised oxygen (50% or 80% as noted) for four days. Controls received either vehicle or room air, as appropriate. All treatment was discontinued after four days and animals were returned to their home cages and maintained at room air with food and water *ad libitum*.

Tissue Collection and Histological Examination

At termination, all animals were deeply anaesthetised (3% isoflurane) and transcardially perfused with paraformaldehyde (4% in 0.15M phosphate buffer). In some animals, pimonidazole (60 mg/kg; i.v.) was administered four hours prior to perfusion to assess tissue oxygenation. The spinal cord at the site of the injection was removed and post-fixed in 4% paraformaldehyde overnight, prior to cryoprotection and snap freezing in liquid nitrogen/isopentane. For histochemical examination of mitochondrial complex activity, some animals were transcardially perfused with cold, oxygenated rinse solution alone, and the fresh tissue was removed and snap frozen as above. Lesions were collected from animals in matched pairs (treatment and control).

For (immuno)histochemical examination, fixed cryosections were examined at the lesion epicentre using standard techniques and a range of stains and antibodies (Supplementary Tables

1 & 2). Images were obtained using standard light and confocal microscopes. All analysis and quantification was performed blind using ImageJ.

In some experiments, lesion volumes were assessed by studying excised spinal cords positioned in a 9.4T preclinical MRI scanner.

Mitochondrial Studies

Mitochondrial biogenesis was assessed following the intraperitoneal administration of bromodeoxyuridine (200mg/ml; 5ml/kg). Control animals were injected with saline. At termination, tissues were fixed by perfusion as described above and mitochondrial biogenesis revealed by immunohistochemistry.

Histochemical study of mitochondrial complex IV was conducted as previously described[14].

Methods are described in detail in the supplementary document.

Results

The lesion and associated disability were found to evolve over three phases (Figure 1A). First, an acute inflammatory lesion (days 1-4) accompanied by significant ($p<0.0001$) relapse-like hindlimb and tail weakness. Second, a period of remission as the inflammation subsided and function was restored. Finally, the onset of progressive significant disability ($p<0.0001$) that evolved over the lifetime in step with progressive atrophy of the previously affected grey matter (Figure 2A). The eventual disability exceeded that observed acutely. Saline-injected control animals showed no such changes.

The progressive atrophy commenced within a month of the initial inflammatory lesion, which focused attention on events in the acute lesion that may be responsible. Histological examination of the acute lesion revealed prominent activation and recruitment of

microglia/macrophages in the grey matter on the lesioned side of the spinal cord (Figure 1Bi & ii; Supplementary Fig. 1B), which was most intense on days 2-3 post-injection, coinciding with the acute peak in disability. At this time the inflamed tissue was noticeably hypoxic, as indicated by significant immuno-labelling for pimonidazole ($p=<0.001$) (Figure 1Fi; Supplementary Fig. 1C) and hypoxia inducible factor-1α (HIF-1 α; $p<0.05$) (Figure 1Fii; Supplementary Fig. 1D). The BBB on the side ipsilateral to the lesion was acutely significantly compromised (Figure 1C; Supplementary Fig. 1E) ($p<0.001$, compared with the contralateral side; $p<0.05$, compared with saline-injected controls). The hypoxic tissue showed increased labelling for superoxide/ROS (Figure 1D), apparently within mitochondria (Figure 1D, inset). Notably, the rise in superoxide/ROS was coupled at 2-3 days with the significant unilateral expression of the inducible form of nitric oxide synthase, and thus of nitric oxide (Figure 1Gi & ii; Supplementary Fig. 1F) ($p<0.001$, compared with the contralateral side; $p<0.05$, compared with saline-injected controls), and the inevitable formation (with superoxide) of peroxynitrite[15]. Superoxide, nitric oxide and peroxynitrite all impair mitochondrial function[16], and this was evidenced in motor neurons by a significant decrease of 63% on day 2 of the ratio of the histochemical activity of mitochondrial complex IV (the oxygen-binding complex) and the immunohistological labelling for the catalytic COX1 subunit of complex IV (Figure 1Ei; see also Supplementary Fig. 1G) ($p<0.01$), denoting impaired mitochondrial function. The maximal mitochondrial impairment on day two precisely coincided with the peak of acute disability (Figure 1A) and impaired electrical excitability of motoneurons (Figure 1Eii & iii). The fall in mitochondrial function and presumed tissue energy crisis was promptly (days two and three) followed by a marked (120%) increase in mitochondrial biogenesis[17] (Figure 1Eiv) and a clear unilateral increase in abundance of mitochondria (Figure 1Ev). The acute inflammation and hypoxia substantially subsided by day four, coincident with the onset of remission and the return of near normal function, which persisted for approximately two weeks.

The period of remission was followed by the third phase of lesion development characterised by the degeneration of motor neurons (Figure 2B) ($p<0.0001$) and the slowly progressive atrophy of the previously inflamed spinal grey matter (Figure 2A, Ci & ii) ($p<0.001$). The degeneration occurred in association with significant focal accumulation of astrocytes (Figure 2Di & ii) ($p<0.01$) and significant activation of ($iNOS^-$) microglia/macrophages (Figure 2Ei & ii) ($p<0.01$), and, notably, the tissue undergoing atrophy showed mitochondrial damage manifest as a deficiency of the activity of mitochondrial respiratory complex IV (Figure 2Fii).

The advancing atrophy occurred hand in hand with the gradual return of significant disability over the lifetime, manifest as a limp and other gait abnormalities in the hindlimb ipsilateral to the lesion (Figure 3Ciii; Supplementary Fig. 1I & Jii) ($p<0.05$), coupled with weakness of the tail (Figure 1A) ($p<0.0001$).

Animals treated with nimodipine or oxygen for the first four days following lesion induction showed a significant reduction in the first, acute phase of disability (Figure 3A, Bi & ii; Supplementary Fig. 1A; oxygen $p<0.01$; nimodipine $p<0.05$). Although reducing disability, there was no significant difference in the magnitude of acute inflammation, as judged by the abundance of microglia/macrophages (Supplementary Fig. 1H), or their amoeboid, activated morphology (not shown). Even though the treatments were applied for just the first four days following lesion induction, treated animals showed a significant protection from not only the acute disability, but also significant protection from the subsequent lifetime of progressive disability (Figure 3A; oxygen $p<0.01$; nimodipine $p<0.05$; Figure 3Ciii; Supplementary Fig. 1A; nimodipine $p<0.0001$; oxygen $p<0.01$), and grey matter atrophy (Figure 3Ci, ii, iv & v; Supplementary Fig. 1Ji) (oxygen $p<0.05$ and $p<0.01$, nimodipine $p<0.01$ and $p<0.05$). In untreated animals the acute and chronic disability was sufficiently severe to be apparent upon simple visual inspection of freely walking animals, but in animals treated with nimodipine or oxygen any disability was subtle, with no significant difference, in e.g. balance (Supplementary Fig. 1I) or swing speed (Supplementary Fig. 1Jii), between the legs ipsilateral and contralateral to the lesion. Animals treated with nimodipine naturally walked significantly faster than untreated controls at 6 months ($p<0.05$) (oxygen $p=0.054$) (Figure 3Ciii).

Discussion

The results describe an acute neuroinflammatory lesion in young adulthood that not only causes acute disability comparable to a relapse in MS, followed by remission, but is followed by a lifetime of slowly progressive disability. The progressive disability occurs in parallel with advancing neurodegeneration and atrophy of the previously inflamed tissue. The tissue undergoing progressive atrophy is characterised by astrocytic and microglial/macrophage activation and a loss of activity of mitochondrial complex IV, as occurs in MS[18]. The acutely inflamed lesion is profoundly hypoxic, and treatment with nimodipine or oxygen (known to

prevent hypoxia in another neuroinflammatory lesion[9,11]), not only significantly reduces the acute disability, but, importantly, it also significantly reduces the chronic, progressive disability. In fact, whereas in untreated animals the acute and chronic disability was sufficiently severe to be apparent upon simple visual inspection of freely walking animals (a level of disability that may prompt use of a walking stick in humans), in animals treated with nimodipine or oxygen any disability was subtle with no significant difference, in e.g. swing speed, between the legs ipsilateral and contralateral to the lesion.

Considering mechanisms, the hypoxia of the acutely inflamed tissue appears key to several features of the lesion. The hypoxia will, for example, contribute to mitochondrial failure and thus to the acute disability, as it does in experimental autoimmune encephalomyelitis (EAE, a common model of MS)[9,11,19,20]. Indeed, the hypoxia appears to be a main cause of the acute disability given that the disability is significantly reduced by treatment with vasodilating nimodipine, or oxygen. The hypoxia will also promote other features of the lesion, including the formation of the observed microglial/macrophage activation[21] and BBB breakdown[22], and the production of ROS[23] and nitric oxide[24], and hence the production of the peroxynitrite[15] that can damage mitochondrial complexes and DNA[25]. Thus the hypoxia lies as a root cause of several factors that synergise to create a particularly toxic cellular environment[26], and one that is particularly deleterious for oxidative mitochondrial metabolism[27]. The consequent shortage of ATP will depolarise neurons, significantly reducing their excitability as observed, and resulting in the observed neurological deficits. In common with EAE[9,11,12], it appears that the hypoxia is not sufficiently severe to kill the neurons and other cells, and when the inflammation subsides and oxygenation increases the cells resume functioning and remission commences.

The chronic, slowly progressive accumulation of permanent disability can be attributed to the slowly progressive neurodegeneration and grey matter atrophy that accompanies it, but why the cells degenerate is uncertain. The fact that the degeneration is significantly reduced by treatment with nimodipine or oxygen restricted to the first four days of lesion development appears to pinpoint the seeds of the damage being sown within the acutely inflamed hypoxic lesion during young adulthood. Nimodipine has a range of potentially valuable neuroprotective properties that may be involved[28,29], but the fact that oxygen is similarly protective focuses

attention on the vasodilatory effects of nimodipine which, like inspiratory oxygen, will improve tissue oxygenation and overcome the hypoxia.

If the damage is inflicted in the acute hypoxic lesion in early adulthood it implies the existence of a cellular mechanism capable of storing the 'memory' of the earlier event over time, while the cells continue functioning. A mechanism that fits the available evidence derives from the cascade described above in which hypoxia promotes a toxic environment including the excessive production of mitochondrial superoxide, nitric oxide and peroxynitrite. Peroxynitrite, in particular, can damage mitochondrial complex IV[27] and the mitochondrial DNA (mtDNA)[25] responsible for the production of functioning complex IV (and other essential mitochondrial constituents), consistent with the loss of mitochondrial complex IV activity observed in the tissue undergoing atrophy. Indeed, the toxic environment for mitochondria occurs at precisely the time of the dramatic increase in mitochondrial biogenesis and mtDNA replication on days two and three following LPS injection, and thus the newly forming mtDNA is likely to be damaged. Replication of the damaged mtDNA over time as mitochondria proliferate will increase heteroplasmy, eventually reaching a lethal point where the cells lack sufficient capacity for oxidative phosphorylation. Thus, it appears that the cellular 'memory' of the acute damage in young adulthood may be stored as permanent damage to the cellular mtDNA.

It is interesting that the eventual disability exceeds that observed acutely, indicating that the tissue undergoing neurodegeneration and atrophy includes tissue that continued functioning throughout the period of acute inflammation. This observation suggests that the mechanisms responsible for the degeneration can be established in the absence of preceding deficits, raising the possibility that tissue can remain functioning and asymptomatic despite having been mortally damaged. The mechanisms involved may help to explain the 'progression independent of relapsing activity' (PIRA) described in progressive MS[30] and other neurodegenerative diseases that arise in later life without preceding neurological deficits.

In summary, the findings show that inflamed hypoxic lesions in young adulthood not only cause acute neurological deficits that diminish as the inflammation and hypoxia subside, but the hypoxic inflamed lesions also covertly 'doom' the affected tissue to eventual degeneration over the lifetime, in association with a loss of activity of mitochondrial complex IV. The acute

and chronic disability, and progressive degeneration and atrophy are all significantly reduced by either of two strategies that protect the inflamed tissue from the associated acute hypoxia. It is intriguing that just a few days of inflammatory hypoxia in young adulthood can inflict occult damage that resonates over the lifetime. Additionally, that treatment that protects from hypoxia for just these few days provides significant lifelong protection. It is encouraging that avoiding inflammatory hypoxia provides a relatively simple route to a treatment achieving both acute and chronic neuroprotection.

Data availability

The data are available upon reasonable request to the corresponding author.

Funding

We acknowledge funding from the International Progressive Multiple Sclerosis Alliance (to KJS and DM), Medical Research Council, UK, Multiple Sclerosis Society, UK, and the National Multiple Sclerosis Society, USA, to KJS. LS was supported by the Deutsche Forschungsgemeinschaft (GRK2727, SCHI 1330/11-1, FOR 5705: SCHI 1330/13-1, SPP 2395: SCHI 1330/10-1), the National Multiple Sclerosis Society PA-2301-40697, the European Research Council (DecOmPress ERC StG, No 950584), and the Hertie Foundation (P1180016).

Competing interests

The authors declare no competing interests.

Supplementary material

Supplementary material is available at *Brain* online.

References

1. Lassmann H. Mechanisms of neurodegeneration shared between multiple sclerosis and Alzheimer's disease. *J Neural Transm*. 5/2011 2011;118(5):747-752. doi:10.1007/s00702-011-0607-8 [doi]

2. Lassmann H. The contribution of neuropathology to multiple sclerosis research. *Eur J Neurol*. Sep 2022;29(9):2869-2877. doi:10.1111/ene.15360

3. Adingupu DD, Evans T, Soroush A, *et al*. Temporal pattern of cortical hypoxia in multiple sclerosis and Its significance on neuropsychological and clinical measures of disability. *Ann Neurol*. Dec 2023;94(6):1067-1079. doi:10.1002/ana.26769

4. Campbell G, Mahad DJ. Mitochondrial dysfunction and axon degeneration in progressive multiple sclerosis. *FEBS Lett*. Apr 2018;592(7):1113-1121. doi:10.1002/1873-3468.13013

5. Waldman AD, Catania C, Pisa M, Jenkinson M, Lenardo MJ, DeLuca GC. The prevalence and topography of spinal cord demyelination in multiple sclerosis: a retrospective study. *Acta Neuropathol*. Mar 9 2024;147(1):51. doi:10.1007/s00401-024-02700-6

6. Yang R, Dunn JF. Reduced cortical microvascular oxygenation in multiple sclerosis: a blinded, case-controlled study using a novel quantitative near-infrared spectroscopy method. *Sci Rep*. 2015 2015;5:16477. doi:srep16477 [pii];10.1038/srep16477 [doi]

7. Geurts JJ, Calabrese M, Fisher E, Rudick RA. Measurement and clinical effect of grey matter pathology in multiple sclerosis. *Lancet Neurol*. Dec 2012;11(12):1082-92. doi:10.1016/S1474-4422(12)70230-2

8. Schlaeger R, Papinutto N, Panara V, *et al*. Spinal cord gray matter atrophy correlates with multiple sclerosis disability. *Ann Neurol*. Oct 2014;76(4):568-80. doi:10.1002/ana.24241

9. Desai RA, Davies AL, Del Rossi N, *et al*. Nimodipine reduces dysfunction and demyelination in models of multiple sclerosis. *Ann Neurol*. Jul 2020;88(1):123-136. doi:10.1002/ana.25749

10. Desai RA, Davies AL, Tachrount M, *et al*. Cause and prevention of demyelination in a model multiple sclerosis lesion. *Ann Neurol*. 1/27/2016 2016;79:591-604. doi:10.1002/ana.24607 [doi]

11. Davies AL, Desai RA, Bloomfield PS, *et al*. Neurological deficits caused by tissue hypoxia in neuroinflammatory disease. *Ann Neurol*. 12/2013 2013;74(6):815-825. doi:10.1002/ana.24006 [doi]

12. Amatruda M, Harris K, Matis A, *et al*. Oxygen treatment reduces neurological deficits and demyelination in two animal models of multiple sclerosis. *Neuropathol Appl Neurobiol*. Dec 15 2023;49:e12868. doi:10.1111/nan.12868

13. Felts PA, Woolston AM, Fernando HB, *et al*. Inflammation and primary demyelination induced by the intraspinal injection of lipopolysaccharide. *Brain*. 7/2005 2005;128(Pt 7):1649-1666.

14. Campbell GR, Mahad DJ. A Method to Detect Cytochrome c Oxidase Activity and Mitochondrial Proteins in Oligodendrocytes. *Methods Mol Biol*. 2019;1936:333-342. doi:10.1007/978-1-4939-9072-6_19

15. Beckman JS, Koppenol WH. Nitric oxide, superoxide, and peroxynitrite: the good, the bad, and the ugly. . *American Journal of Physiology*. 11/1996 1996;271(5 Pt 1):C1424-C1437.

16. Brown GC, Borutaite V. Nitric oxide inhibition of mitochondrial respiration and its role in cell death. *Free Radical Biology & Medicine*. 12/1/2002 2002;33(11):1440-1450.

17. Gutsaeva DR, Carraway MS, Suliman HB, *et al*. Transient hypoxia stimulates mitochondrial biogenesis in brain subcortex by a neuronal nitric oxide synthase-dependent mechanism. *J Neurosci*. 2/27/2008 2008;28(9):2015-2024. doi:28/9/2015 [pii];10.1523/JNEUROSCI.5654-07.2008 [doi]

18. Campbell GR, Kraytsberg Y, Krishnan KJ, *et al*. Clonally expanded mitochondrial DNA deletions within the choroid plexus in multiple sclerosis. *Acta Neuropathol*. 8/2012 2012;124(2):209-220. doi:10.1007/s00401-012-1001-9 [doi]

19. Nikic I, Merkler D, Sorbara C, *et al*. A reversible form of axon damage in experimental autoimmune encephalomyelitis and multiple sclerosis. *Nat Med*. 3/27/2011 2011;17:495-499. doi:nm.2324 [pii];10.1038/nm.2324 [doi]

20. Sadeghian M, Mastrolia V, Haddad AR, *et al*. Mitochondrial dysfunction is an important cause of neurological deficits in an inflammatory model of multiple sclerosis. *Scientific Reports*. 2016 2016;6:33249.

21. Butturini E, Boriero D, Carcereri de Prati A, Mariotto S. STAT1 drives M1 microglia activation and neuroinflammation under hypoxia. *Arch Biochem Biophys*. Jul 15 2019;669:22-30. doi:10.1016/j.abb.2019.05.011

22. Engelhardt S, Al-Ahmad AJ, Gassmann M, Ogunshola OO. Hypoxia selectively disrupts brain microvascular endothelial tight junction complexes through a hypoxia-inducible factor-1 (HIF-1) dependent mechanism. *J Cell Physiol*. 8/2014 2014;229(8):1096-1105. doi:10.1002/jcp.24544 [doi]

23. Robinson MA, Baumgardner JE, Otto CM. Oxygen-dependent regulation of nitric oxide production by inducible nitric oxide synthase. *Free Radic Biol Med*. Dec 1 2011;51(11):1952-65. doi:10.1016/j.freeradbiomed.2011.08.034

24. Robinson MA, Baumgardner JE, Otto CM. Oxygen-dependent regulation of nitric oxide production by inducible nitric oxide synthase. *Free Radic Biol Med*. 12/1/2011 2011;51(11):1952-1965. doi:S0891-5849(11)00547-8 [pii];10.1016/j.freeradbiomed.2011.08.034 [doi]

25. Calcerrada P, Peluffo G, Radi R. Nitric oxide-derived oxidants with a focus on peroxynitrite: molecular targets, cellular responses and therapeutic implications. *Curr Pharm Des*. Dec 2011;17(35):3905-32. doi:10.2174/138161211798357719

26. Brown GC, Neher JJ. Inflammatory neurodegeneration and mechanisms of microglial killing of neurons. *Mol Neurobiol*. 6/2010 2010;41(2-3):242-247. doi:10.1007/s12035-010-8105-9 [doi]

27. Parihar A, Vaccaro P, Ghafourifar P. Nitric oxide irreversibly inhibits cytochrome oxidase at low oxygen concentrations: evidence for inverse oxygen concentration-dependent peroxynitrite formation. *Iubmb Life*. 1/2008 2008;60(1):64-67. doi:10.1002/iub.12 [doi]

28. Frank R, Szarvas PA, Pesti I, *et al*. Nimodipine inhibits spreading depolarization, ischemic injury, and neuroinflammation in mouse live brain slice preparations. *Eur J Pharmacol*. Jun 6 2024;977:176718. doi:10.1016/j.ejphar.2024.176718

29. Hohmann U, Ghadban C, Hohmann T, *et al*. Nimodipine Exerts Time-Dependent Neuroprotective Effect after Excitotoxical Damage in Organotypic Slice Cultures. *Int J Mol Sci*. Mar 19 2022;23(6)doi:10.3390/ijms23063331

30. Portaccio E, Betti M, De Meo E, *et al*. Progression independent of relapse activity in relapsing multiple sclerosis: impact and relationship with secondary progression. *J Neurol*. May 28 2024;doi:10.1007/s00415-024-12448-4

Figure legends

Figure 1 Progression of the lesion: disability and acute histological and electrophysiological findings. A. Course of disability observed while rats are walking on a horizontal surface for 1 metre, showing a significant difference between animals injected with LPS (n=20, red) vs. saline (n=10, green) ($p<0.0001$). Rats normally walk with raised tail (score 0), but weakness causes the distal tail to droop and touch the ground (score 1.5) or the whole tail can become flaccid (score 3). Mean ± SEM, $p<0.0001$. Two-way ANOVA with Bonferroni correction for multiple comparisons. B-G and Ev. Histological images showing transverse sections through the spinal cord at the level of an intraspinal injection made into the left side as shown. Bi & ii. The lesioned tissue is characterised by raised microglial/macrophage activation on the lesioned side, marked by immunolabelling for IBA1 (Bi) and ED1 (Bii) two days post-injection (dpi) of LPS. Fi & ii. The lesion is acutely hypoxic, indicated by immunolabelling for pimonidazole (Fi) and hypoxia inducible factor-1a (HIF1a) (Fii) at 3dpi. C. There is breakdown of the blood-brain barrier largely confined to the lesioned side, marked by immunolabelling for fibrinogen 3dpi. D. The lesion shows raised production of superoxide, indicated by dihydroethidium fluorescence at 3dpi) which is especially prominent in ventral horn motor neurons (upper inset) and in clusters of mitochondria within such neurons (lower inset shows a single motor neuron (outlined)). Gi & iiI. The lesioned side shows marked expression of cells immunolabelled for inducible nitric oxide synthase (iNOS; red) and ED1 (green) at 1dpi, indicating raised production of nitric oxide especially in activated microglia/macrophages (appearing yellow). $iNOS^+$ cells are rare on the contralateral side in LPS-lesioned tissue, and absent from control spinal cords injected with saline (Gii). The free radicals superoxide and nitric oxide will avidly combine to form peroxynitrite, and all these three factors impair mitochondrial function, which will be accentuated by the hypoxia. Ei. Bar graph showing the corresponding significant impairment of mitochondrial function in motor neurons during the first four days, indicated by changes in the ratio of histochemical reactivity of the mitochondrial complex IV (COX) and the immunoreactivity of the catalytic COX complex I. Data points indicate individual animals.

Mean ± SD, one-way ANOVA. Eii & iii. The depression of mitochondrial function correlates with a depression of the excitability of motor neurons, manifest as a reduction in the ratio of the electromyographic F wave compared with the directly conducted M response over time (Eii), and a reduction in the ratio of the electromyographic H reflex compared with the directly conducted M response over time (Eiii), both of which provide a measure of the excitability of ventral horn motor neurons. Excitability is significantly depressed ($p<0.001$ (Eii) and $p<0.05$ (Eiii)) at 2dpi, when mitochondrial function is also significantly depressed (Figure. Ei). Eiv. The depression of mitochondrial function on days 2-3 is accompanied by a significant ($p<0.01$) increase in mitochondrial proliferation on days 2-3 indicated by increased BrDU labelling of mitochondrial DNA. Mean ± SD; one-way ANOVA, with Dunnett's correction for multiple comparisons. Ev. The marked increase in mitochondrial proliferation is associated with a marked increase in mitochondrial density on the lesioned side, indicated by immunolabelling for mitochondrial porin at 3dpi). * $p<0.05$; ** $p<0.01$; *** $p<0.001$; **** $p<0.0001$. Scale bars: 500μm in Bi & ii, C, D, Ev,Fi, Gi; 100μm in Fii & Gii.

Figure 2 Progression of the lesion: chronic findings. A. Graph showing the increasing atrophy of the grey matter at the lesion site, comparing ipsilateral vs. contralateral sides, and injections of LPS vs. saline. LPS: 1m (n=3), 3m (n=3), 6m (n=4) and 12m (n=12). T-test, p=0.006. B. Graph demonstrating significant loss of motor neurons at 12 months, comparing animals injected with LPS (n=8) vs. saline (n=6). Mean ± SD, t-test, p=0.0001. Ci & Di. Illustrations showing atrophy of the ipsilateral ventral horn. Ci. Transverse H&E section through an LPS lesion at 12 months illustrating marked atrophy of the ipsilateral grey matter (grey matter boundary outlined in yellow). Cii. Graph showing significant atrophy of the ipsilateral ventral horn at 7 months in animals injected with LPS vs. saline. Independent t-test ($p<0.001$). Di & Dii. Illustrations showing astrogliosis at the site of injection of LPS. Di. Transverse section from a spinal cord injected with LPS 12 months previously, showing immunolabelling for glial fibrillary acidic protein (GFAP). Dii. Graph showing significantly increased immunolabelling for GFAP ipsilateral to the site of injection, and compared with saline-injected controls. Independent t-test ($p<0.01$). Ei & ii. Illustrations showing concentration and activation of microglia/macrophages in chronic lesions at the site of LPS injection. Ei. Transverse section from spinal cord injected with LPS 12 months previously, showing immunolabelling for IBA1, a marker of microglia/macrophages. Eii. Graph showing

significantly increased immunolabelling for IBA1 ipsilateral to the site of injection, and compared with saline-injected controls. LPS vs. ipsilateral saline, independent t-test ($p<0.01$); LPS ipsilateral vs contralateral, paired t-test ($p<0.01$). Fi & ii. Transverse sections from saline- and LPS-injected spinal cords showing histochemistry for mitochondrial complex IV activity, 12 months post-injection. The grey matter boundary is indicated in yellow. Note the lack of complex IV activity in the grey matter undergoing atrophy (outlined in red). The injections in Ci, Di, Ei & F were positioned more superficially in the spinal cord than in most other figures. Scale bars: 500μm in Ci, Di, Ei and Fi & ii.

Figure 3 Protection by treatments that prevent lesion hypoxia. A. Course of disability comparing animals injected with LPS and treated for only the first 4 days with either nimodipine (n=23), 80% inspiratory oxygen (n=23), or no treatment (n=23). The pink band marks the severity of disability that is easily detected by visual observation while rats are walking on a level surface. Note that untreated animals spend much of their time in the pink region, but treated animals are never this severely affected. Mean ± SEM; one-way ANOVA, Dunnett's multiple comparisons test; hyperoxia, $p=0.0045$, nimodipine $p=0.0362$. Bi. Detail from Figure 3A. Mean ± SEM; two-way ANOVA, Dunnett's multiple comparisons test; hyperoxia, $p<0.01$; nimodipine $p<0.01$. Bii. Graph showing hindlimb disability marked by slips of the right foot while walking along a horizontal ladder, for animals injected with LPS into the right ventral horn and either treated with nimodipine (n=24) or vehicle (control; n=15). Animals treated with nimodipine walked significantly better than untreated animals two days after LPS injection. Animals were trained from 1 day before surgery (baseline) up to four days after surgery. Two-way ANOVA, $p<0.001$. Values are means +/- SEM. Ci & ii. Transverse sections through the spinal cord at the level of lesions induced 12 months previously, comparing vehicle control treatment (same as Figure 2Ci) with protective treatment for the first four days alone with nimodipine. The border of the grey matter is outlined in yellow. Nimodipine treatment protects from grey matter atrophy. Scale bars 500μm. Ciii. Graph showing the walking speeds of rats freely walking on a flat surface recorded by video camera six months after LPS injection, comparing untreated control animals with those acutely treated (for 4 days) with inspiratory 80% oxygen, or nimodipine. Rats treated with nimodipine walked significantly faster than untreated animals. Mean ± SEM; independent t-test; $p<0.05$. Civ & v. Bar graphs showing significant protection from grey matter atrophy at 12 months following LPS injection, mediated by acute (4 days)

treatment with (Civ) 50% or 80% inspiratory oxygen (room air controls n=11; 50% oxygen n=8; 80% oxygen n=7) (atrophy determined from H&E sections comparing lesioned tissue with vehicle controls; $p<0.05$) or (Cv) acute (4 days) treatment with nimodipine (n=16) vs. vehicle controls (n=8) (grey matter volume determined by MRI; mean ± SD; one-way ANOVA; mean ± SD, t-test; $p<0.01$).

Supplementary Figure 1

A. Graph showing the progression of disability over a year for animals intraspinally injected with LPS and tested while walking on a horizontal surface for 1 metre, during acute and chronic periods. Animals receiving no treatment (n=11) show significantly greater disability than animals acutely treated (for 4 days) with either inspiratory 80% oxygen (n=10) or nimodipine (n=18). Animals were tested before injection, for four consecutive days after injection, and then monthly. Data show a separate trial from that illustrated in Fig. 3A. Mean SEM; one-way ANOVA, Dunn's multiple comparisons test, hyperoxia p=0.0031, nimodipine p<0.0001.

B. Graph showing the area occupied by activated $ED1^+$ microglia/macrophages two days after intraspinal LPS injection vs. saline control injection, comparing the ipsilateral and contralateral ventral grey matter. The ipsilateral ventral grey matter injected with LPS contained significantly more activated microglia/macrophages than either the contralateral grey matter or the grey matter of saline injected controls. Ipsilateral saline vs LPS = independent t test, p<0.001; LPS ipsilateral vs contralateral = paired t test p<0.001.

C. Graph showing the relative intensity of tissue hypoxia marked by immunolabelling for pimonidazole, comparing the ventral grey matter of the spinal cord ipsilateral to an injection of either LPS or saline (control) one to four days previously. The LPS-injected spinal cord labels significantly more intensely for hypoxia than control spinal cord two days following injection. Independent t test, p<0.001.

D. Graph showing the relative intensity of tissue hypoxia marked by immunolabelling for hypoxia inducible factor-1a (HIF1a), comparing the ventral grey matter of the spinal cord ipsilateral to an injection of either LPS or saline (control) two days previously. The LPS-injected spinal cord labels significantly more intensely for hypoxia than control spinal cord. Independent t test, p<0.05.

E. Graph showing breakdown of the BBB marked by immunolabelling for fibrinogen, comparing the spinal grey matter ipsilateral and contralateral to an injection of either LPS or saline (control) two days previously. The spinal cord ipsilateral to the LPS injection labels significantly more intensely for fibrinogen than the contralateral side of the same animals (p<0.001), and significantly more intensely than saline-injected controls (p<0.05). Ipsilateral saline vs LPS = independent t test; LPS ipsilateral vs contralateral = paired t test.

F. Graph showing the area occupied by immunolabelling for the inducible form of nitric oxide synthase (iNOS), comparing the spinal ventral grey matter ipsilateral and contralateral to an injection of either LPS or saline (control) two days previously. The spinal cord ipsilateral to the LPS injection labels significantly more intensely for iNOS than the contralateral side of the same animals ($p<0.01$), and significantly more intensely than saline-injected controls ($p<0.05$). Ipsilateral saline vs LPS = independent t test; LPS ipsilateral vs contralateral = paired t test.

G. Images showing COX activity and COX-I immunoreactivity in the ventral horn of a control animal (Gi) and the ventral horn of an animal injected with LPS (Gii). Red labelling indicates complex IV activity in the ventral horn, judged by COX histochemistry. Green labelling indicates immunoreactivity of the complex IV subunit-I (COX-I) in mitochondria, in particular mitochondria that lack complex IV activity, following sequential COX histochemistry/COX-I immunohistochemistry as previously described (Mahad et al., J. Neurosci. Methods 2009;184:310-319). Ventral horn neurons abundant in complex IV activity are present in control tissue (red and minimal green labelling) whereas complex IV is deficient in the LPS-injected ventral horn (minimal red and mostly green labelling). Arrowheads indicate ventral horn neuronal cell bodies.

H. Bar graph showing lack of effect of acute treatment with 80% oxygen or nimodipine in preventing acute inflammation, as indicated by immunolabeling for IBA1. Mean □ SD; one-way ANOVA, no statistical significance.

I. Gait analysis showing the balance between the hindlimbs two days after the intraspinal injection of LPS. In placebo-treated animals the function of the hindlimb ipsilateral to the lesion was significantly worse than that of the contralateral limb (i.e. gait balance significantly below zero), but the function of the ipsilateral leg was protected in animals acutely treated with either 80% oxygen or nimodipine for 4 days (i.e. function in the ipsilateral hindlimb was not significantly different from that of the contralateral hindlimb). Mean □ SEM; one-way ANOVA, Dunn's multiple comparisons test, no statistical significance.

Ji. The length of the lesion assessed by MRI examination one year after induction, comparing lesions in the absence of neuroprotective treatment (n=14), and after acute (four days) treatment with inspiratory oxygen (80%) (n=7) or nimodipine (n=16). Lesions are

significantly shorter in treated animals (hyperoxia p=0.0037; nimodipine p=0.0235). Mean □SD; two-way ANOVA, Dunnett's multiple comparisons test.

Jii. Gait analysis showing the swing speed scores for the hindlimbs ipsilateral and contralateral to an LPS lesion induced 6 months previously. Lines connect the legs of individual animals, grouped into no treatment, and acute treatment with nimodipine or 80% oxygen for the first 4 dpi. The swing speed was significantly slower on the ipsilateral side with no treatment, but either treatment provided protection (i.e. no significant difference between sides). Paired t-test; p=0.0270.

Online Supplementary text

Methods

Lesion Induction – Intraspinal LPS injection

A quarter laminectomy was performed aseptically between the T13 and L1 vertebrae in adult male Sprague Dawley rats (323.3+-48.7g, mean ± standard deviation), under deep isoflurane (Merail, Harlow, UK) anaesthesia (1.5-2% in room air). A glass micropipette was used to microinject lipopolysaccharide (LPS; 0.5 µl of 80 ng/µl in saline; *Salmonella enterica*, serotype typhimurium, Sigma-Aldrich, St Louis, MO) into the right ventral horn, positioned 700 µm lateral from the midline, at depths of 1100 and 1300 µm. Control animals received similar injections of saline alone. The injection site was marked with powdered charcoal on the dura for subsequent histological localisation.

We have chosen LPS as a pro-inflammatory agent because even in healthy humans, microglia are daily 'irritated and aggravated' by leakage into the brain of low levels of naturally circulating LPS, which contribute to a chronic state of low-grade neuroinflammation[1,2]. LPS is therefore a factor to be considered in the context of MS, especially where the blood-brain barrier is disturbed.

Assessment of neurological deficit

Video recordings were made of animals walking freely and voluntarily on a level surface to evaluate the function of the tail and hindlimbs at the following timepoints; before lesion induction, and at 1, 2, 3, 4, 7, and 14 days, and then monthly until termination at 6 or 12 months after lesion induction. Neurological function was assessed by gait analysis and by measuring tail elevation.

Gait Analysis

Gait analysis was assessed using established methods[3]. For each animal at each timepoint, a video recording was considered valid if the animal walked with steady speed for at least four consecutive steps. From this walk, stride length was measured, and stance and swing times were measured for both left and right hindlimbs. The percent stance time (i.e. duty factor) was calculated as stance time divided by stride time (duty factor = stance time / stride time), and balance between left and right hindlimbs as the duty factor of right hindlimb minus the duty factor of left hindlimb (balance = duty factor right - duty factor left). Additionally, swing speed was calculated as stride length divided by swing time (swing speed = stride length / swing time), stride speed as stride length divided by stride time (stride speed = stride length / stride time), and running speed as an average of the stride speed of both hindlimbs.

Tail Elevation

The magnitude of voluntary tail elevation while walking was quantified using a customised scoring system modified from MacKenzie et al[4]. In brief, an overall score of tail elevation was awarded by observation of the video recorded for each animal at each timepoint, then a representative frame of the video was captured and used to measure the elevation of the tail tip and mid tail from tail base to adjust the overall score awarded from the video, if necessary. A higher score represents less tail elevation, indicating worse motor function.

Illustrations in Figures 3Bii and 3Ciii, and in Suppl. Figures I and Jii describe deficits in hindleg function, and Figures 1A and 3A, and Suppl. Figure A show deficits in tail function.

Treatment

Animals were randomised into groups prior to lesion induction, and treated for the first four days with nimodipine, or inspiratory normobaric oxygen (50% or 80% as noted), or vehicle or room air. For treatment with nimodipine, lesions were induced as described above and immediately following surgery the animals received an intraperitoneal (i.p.) injection of nimodipine (30mg/kg) or vehicle (ethanol:PEG400), and allowed to recover. Treatment with nimodipine (30mg/kg/dose) or vehicle was then maintained by twice daily oral gavage. Animals treated with normobaric oxygen or room air were housed in a chamber containing 50% or 80% (as noted) oxygen for the duration of treatment. All treatment was discontinued after four days, and all animals were returned to their home cages and maintained at room air with food and water *ad libitum* until perfusion in matched pairs (treatment and control).

Perfusion, Tissue Harvesting And Processing For Main (Immuno)-Histological Studies

Pimonidazole (60 mg/kg in saline; HPI Inc, Burlington, MA) was administered systemically via the saphenous vein under temporary light anaesthesia (1.5% isoflurane in room air) four hours prior to terminal perfusion, when required to assess tissue oxygenation. At termination, all animals were deeply anaesthetised (3% isoflurane) and transcardially perfused with rinse solution (0.9% NaCl, 2,000U/l heparin, 0.025% lidocaine, 0.02% 4-[2-hydroxyethyl]-1-piperazineethanesulfonic acid [pH 7.4]) followed by paraformaldehyde (4% in 0.15M phosphate buffer). Spinal cord tissue at the site of the injection was harvested and post-fixed in 4% paraformaldehyde overnight, prior to cryoprotection in 30% sucrose for 48 hours. To allow histochemical examination of the lesion, a subset of animals were transcardially perfused with cold, oxygenated rinse solution alone, and the fresh tissue was snap frozen in liquid nitrogen/isopentane.

Histology and Microscopy

For (immuno)histochemical examination, fixed, 12 µm-thick cryosections were examined at the lesion epicentre using standard techniques and a range of stains and antibodies (Supplementary Tables 1 & 2), as previously described[5]. Tissue labelled using the peroxidase detection system was viewed using an Axiophot light microscope (Carl Zeiss, Oberkochen, Germany) and photographed with a Nikon D300 camera (Nikon Instruments, Melville, NY). Fluorescent images were obtained using a Zeiss LSM5 Pascal or LSM710 confocal microscope, using x10, x20, x40 and x63 objectives.

Histological Quantification

All analysis and quantification was performed blind using ImageJ (NIH, Bethesda, MD). Quantification of ED1, IBA-1, GFAP, fibrinogen, iNOS and other labels was performed by counting the number of pixels above a set threshold, and expressed as the percentage of cross-sectional area coverage. Pimonidazole labelling was quantified as described previously[5]. Analysis of the intensity of the labelling with pimonidazole and HIF1α was carried out by tracing around the spinal cord sections (white and grey matter, and grey matter alone, irrespectively), and measuring the pixel intensity using Image J (National Institute of Health, USA). Quantification of all other markers was carried out using the 'analyse particles' tool, on threshold images, to determine the number of positively labelled cells. The same settings were used for each image, and area measurements were carried out concurrently.

Grey matter atrophy in 2D: Transverse tissue sections stained with haematoxylin and eosin were microscopically examined (Zeiss Axiophot) and photographed (Nikon D300 camera). Grey matter atrophy was calculated by tracing around the area of the ventral horn grey matter on the lesion side and comparing it with the corresponding area on the contralateral side, expressing the result as a percentage relative to the non-lesioned contralateral grey matter. Quantification was carried out using the "analyse measurement" tool of Image J (National Institute of Health, USA).

Grey matter atrophy in 3D (MRI): Fixed spinal cords were washed in phosphate buffered saline prior to arrangement in a series of drinking straws positioned in a custom-built sample holder. The holder was positioned in a 20 cm horizontal 9.4T preclinical MRI scanner (Bruker Biospec, Billerica, MA) equipped with a 40 mm-diameter radiofrequency birdcage volume coil (Bruker Biospec, Billerica, MA). Images were acquired using a 3D fast low angle shot (FLASH) imaging sequence, with a spatial resolution of 30µm x 30µm x 300µm, flip angle 52.0°, matrix size 750 x 750 x 133, repetition time 100ms, time to echo 12ms and number of averages = four. From the images obtained, the cross-sectional area of the grey matter lesion was measured using the selection tool on Image J on each MRI slice where the lesion was visibly present. Subsequently, volume measurements were calculated using the slice thickness and cross-sectional values, where the lesion was visibly present, comparing the lesioned and contralateral sides to deduce the 3D-atrophy volume. A one-way ANOVA test was performed on atrophy volume results to compare the significance between different treatment groups and controls. For treatment groups compared at a single time point, t- tests were performed to assess significance.

Neuronal counts: Sections previously stained with cresyl violet were analysed using ImageJ software (National Institutes of Health, USA). Images of the sections were imported into ImageJ, and relevant regions of interest were identified. Using the cell counter plugin, cells exhibiting morphological features characteristic of motor neurons (such as large soma size, prominent nucleoli, and polygonal shape) were manually identified, counted, and tracked across sections. Counts and measurements were recorded for subsequent statistical analysis. All data were tested for normality using the ShapiroWilk test. A two-way ANOVA test was performed on neuronal counts to assess the significance between different time points

and between the two treatment groups, those being saline and LPS. P-values of 0.05 (*), 0.01 (**), 0.001 (***) and 0.0001(****), were considered as statistically significant. All statistical analyses were carried out using GraphPad Prism version 8.

Statistical analyses were performed with Excel 2010 (Microsoft, USA), Prism 9.0 (GraphPad, USA) or Matlab, using Student's t-test, ANOVA or other related tests. The threshold for statistical significance was indicated as ns ($p>0.05$), * ($p\leq0.05$), ** ($p\leq0.01$), *** ($p\leq0.001$). All descriptive numbers in the text are shown as mean ± standard deviation (SD).

Mitochondrial biogenesis

Mitochondrial biogenesis was assessed as previously described[6]. Bromodeoxyuridine (BrdU) (Sigma-Aldrich, USA) in saline was maintained at 55°C for 30 minutes before intra-peritoneal injection (200mg/ml). The dosing volume was kept constant at 5ml/kg. Control animals were injected with saline. At termination, animals were perfused as described below, except that a piece of small intestine was harvested as a positive control for the BrdU (the inner crypt layer of the intestine undergoes rapid cell proliferation and is a good marker for DNA replication). BrdU was detected using fluorescence immunohistochemistry. Sections were re-fixed with a few drops of 4% PFA for 15 minutes at room temperature before PBS containing 0.3% TritonX-100 for five minutes at ambient temperature, and then the 2N hydrochloric acid for 90 minutes at 40 °C . After washing with PBS, and then PBS containing 0.3% hydrogen peroxide for 10 minutes, followed by two washes with PBS for 5 minutes and then 5% goat serum in PBS with 0.1% tween-20 for one hour. For mouse studies, rat anti-BrdU (MCA2060, AbD Serotec) was used at optimum concentration of 1:200, along with rabbit anti VDAC1 (AbCam) at a concentration of 1:600. Slides were incubated with antibody solutions overnight at 4 °C . The next morning, slides were washed stringently in troughs of PBS with 0.2% tween 3 times, 15 minutes each at room temperature. Secondary antibodies in PBS were applied, biotinylated goat anti rat antibody at 1:200 (Vector labs) and goat anti rabbit conjugated to Alexa fluor 546 (Invitrogen) for 2 hours at room temperature. Slides were washed once again 3 times, each wash lasting 15 minutes with PBS and 0.2% tween. Finally, slides were incubated for 90 min at room temperature with Alexa conjugated Streptavidin (Invitrogen). After a final set of PBS washes, the slides were mounted using Vectashield (Vector labs) and then stored at 4 °C until ready to be imaged.

Images were recorded with Pascal software (Zeiss) and analysed with Image J software (NCBI, USA). Each cell of interest was isolated and analysed individually for BrdU content in BrdU positive mitochondria. A threshold for fluorescence intensity was set manually and kept the same throughout the analysis. A 3D Object counter plug in was used to count the number of mitochondria that were labelled with BrdU. For each cell of interest, a Z project plug in was applied, and the area of BrdU positive particles was calculated per cell.

Tiled images from nerve sections were analysed for BrdU and porin co-localisation using a Coloc2 plug in. The image was split into two colour channels (porin in red and BrdU in green). The threshold was set manually in the red channel, keeping it consistent across all images. Co-localisation analysis was done in 3-dimensions. The level of co-localisation between BrdU-positive and porin-positive particles was presented as an average slope gradient.

Changes in pattern of mitochondrial biogenesis in short-time series experiments were analysed using GraphPad Prism6 software, a one- way ANOVA analysis ($p<0.05$).

Images were recorded with Pascal software (Zeiss) and analysed with Image J software (NCBI, USA). Each cell of interest was isolated and analysed individually for BrdU content in BrdU positive mitochondria. A threshold for fluorescence intensity was set manually and kept the same throughout the analysis. A 3D Object counter plug in was used to count the number of mitochondria that were labelled with BrdU. For each cell of interest, a Z project plug in was applied, and the area of BrdU positive particles was calculated per cell.

Tiled images from nerve sections were analysed for BrdU and porin co-localisation using a Coloc2 plug in. The image was split into two colour channels (porin in red and BrdU in green). The threshold was set manually in the red channel. Co-localisation analysis was done in 3-dimensions. The level of co-localisation between BrdU-positive and porin-positive particles was presented as an average slope

gradient. Changes in pattern of mitochondrial biogenesis in short-time series experiments were analysed using GraphPad Prism6 software, a one-way ANOVA analysis ($p<0.5$).

Methods to detect and quantify mitochondrial complex IV [cytochrome c oxidase (COX)] and its catalytic component (COX-I) immunoreactivity. Combining complex IV histochemistry with immunohistochemistry

The complex IV histochemical reaction was carried out as stated previously[7]. After washing with PBS, immunohistochemistry for COX-1 was conducted by fixation in 4% paraformaldehyde, washing, and applying monoclonal antibodies raised against COX-I (IgG_{2a}; Molecular Probes® Invitrogen Ltd., Paisley, UK). The Menapath X-Cell Plus HRP Polymer detection system (A. Menarini Diagnostics, Wokingham, UK) was used without a blocking step and an optimum concentration of 1:3200 for COX-I primary antibodies. Labelling was detected using the polymer kit as per manufacturing guidelines (A. Menarini Diagnostics, Wokingham, UK). The Vector® SG was used as the HRP substrate and the sections were dehydrated in graded ethanols. Histoclear was applied before mounting in DPX®.

Multi-spectral imaging and densitometric analysis of multiple chromogens:

Bright field images of the two chromogens (diaminobenzidine tetrahydrochloride and Vector® SG) were obtained using the Nuance imaging system (CRi, Woburn, MA), which uses liquid crystal tuneable filters to acquire multi-spectral images and deconvolution methods to separate or 'unmix' the original double labelled image to reveal unmixed images (in grey scale) of each chromogen[8]. The unmixed images may then be used to quantify each chromogen.

The global densitometric values of complex IV activity and immunoreactivity in the entire ventral horns were determined by manually outlining the ventral horns in unmixed images. The single cells with abundant mitochondria, which are mostly neurons based on morphology and NeuN labelling (not shown), were outlined in ventral horns of rat spinal cords by setting a fixed threshold on COX-I immunoreactivity in the sections subjected to immunohistochemistry only. The threshold of COX-I immunoreactivity, which was kept constant, was used to outline the cells abundant in mitochondria in the unmixed images of sections subjected to both complex IV histochemistry and immunohistochemistry. The mean signal and the area of immunoreactivity were recorded within each cell. The outline of cells, based on the immunoreactivity above the threshold, was copied on to the unmixed images of complex IV activity and the mean signal intensity of complex IV histochemistry (activity) was recorded within each corresponding cell.

Discussion

Relevance to neurological disease

We do not advance the new lesion as a precise model of any particular neurological disease, but rather as a tractable model that exhibits mechanisms likely to contribute to the slowly progressive degeneration and atrophy observed in neurological diseases. However, there are notable similarities between the model and progressive MS. In both the model and secondary progressive MS there is i) innate hypoxic neuroinflammation (provoked by LPS in the model, and potentially by acquired immune activity in MS) accompanied by acute disability (relapse) in young adulthood, which undergoes remission, but is ii) followed over the adult lifetime by progressive disability, neurodegeneration and atrophy, which iii) develop in conjunction with astroglial and microglial activation and a deficiency of mitochondrial respiratory complex IV.

The key role of hypoxia is interesting when considered in conjunction with previous observations, because inflammatory tissue hypoxia is emerging as a key cause of both acute and progressive disability and smouldering neurodegeneration and atrophy[this study and 5,9], as well as demyelination[10], all cardinal features of MS. In experimental autoimmune encephalomyelitis (EAE), a commonly used model of MS, hypoxia in the acutely inflamed lesions is sufficient to cause the impairment in mitochondrial function[11], resulting in neuronal inexcitability and disability. Thus, animals dragging their hindlimbs at the onset of inflammatory disease expression in EAE can be restored to strong walking within two hours of breathing normobaric raised oxygen, and the neurological deficits return within one hour of breathing room air[5,9,12].

These dramatic and swift effects in EAE are strongly supportive of a direct effect of tissue hypoxia in impairing mitochondrial function. Impairment by lack of oxygen is probably an important factor in the acute phase of the new model lesion, but the reduction in COX:COX1 activity suggests additional direct damage to mitochondrial complex IV, as may result from the combined effects of hypoxia, nitric oxide and superoxide[12], and the consequent formation of the potent oxidising agent peroxynitrite. Peroxynitrite can cause direct nitration and damage of mitochondrial complex IV[13] and also damage the mitochondrial or nuclear DNA responsible for complex IV formation[14]. The acute neurological deficits probably arise from hypoperfusion of the inflamed tissue, perhaps due in part to raised levels of the potent vasoconstrictive agent endothelin-1, as occurs in MS[15]: nimodipine is a very effective vasodilating antagonist of endothelin-1. Aside from causing neurological deficits, inflammatory tissue hypoxia also causes the Pattern III type of demyelination[12] that occurs in early MS lesions[16], and again strategies that maintain tissue oxygenation provide effective treatments[12]. We conclude that prompt therapy to avoid tissue hypoxia, such as when it is signalled by the onset of new relapses, may achieve significant benefits in MS by reducing both acute and progressive disability.

Aside from MS[17], features including innate immune activation and hypoperfusion precede long term cognitive and other deficits in, e.g. sport-related concussion[18] and boxing[19], traumatic brain injury[20], and Alzheimer's disease[21]. The current findings suggest that precautions to maintain cerebral perfusion and oxygenation, such as those employed in this study, may be important in providing protection from later disability.

Supplementary Table 1- Immunohistochemistry

Antibody	Target	Isotype	Blocking Buffer	Dilution	Source
Mouse Anti-GFAP	Astrocytes	Rabbit IgG	5% normal horse serum (Sigma) in 0.01% PBS-triton-x	1:200	Sigma
Mouse Hydroxyprobe-1-anti-pimonidazole	Pimonidazole adducts	Mouse IgG	0.25% casein (VWR International, UK), in 0.01% PBS- triton-x	1:500	HPI Inc
Mouse Anti-ED1	Activated macrophages/ microglia	Mouse IgG1	5% normal horse serum (Sigma) in 0.01% PBS-triton-x	1:200	Abcam
Rabbit anti-IBA	Macrophages /Microglia	Rabbit IgG	5% normal goat serum (Sigma) in 0.01% PBS-triton-x	1:500	WAKO
Rabbit Anti-HIF-1α	Hypoxia inducible factor-1 α	Rabbit IgG	5% normal goat serum (Sigma) in 0.01% PBS-triton-x	1:200	Abcam

Supplementary Table 2- Immunofluorescence

Antibody	Target	Isotype	Blocking Buffer	Dilution	Source
Rabbit Anti- GFAP	Astrocytes	Rabbit IgG	5% NGS in 0.01% PBS-triton	1:500	DAKO
Rabbit Hydroxyprobe-1-anti-pimonidazole	Pimonidazole adducts	Rabbit IgG	5% NGS in 0.01% PBS-triton	1:500	HPI Inc

Rabbit Anti-IBA	Microglia/ macrophages	Rabbit IgG	5% NGS in 0.01% PBS-triton	1:200	Abcam
Rabbit Anti-fibrinogen	Fibrinogen	Rabbit IgG	5% NGS in 0.01% PBS-triton	1:400	Abcam
Rabbit Anti-iNOS	iNOS	Rabbit IgG	5% NGS in 0.01% PBS-triton	1:100	Invitrogen

1. Sandiego CM, Gallezot JD, Pittman B, *et al*. Imaging robust microglial activation after lipopolysaccharide administration in humans with PET. *Proc Natl Acad Sci U S A*. Oct 6 2015;112(40):12468-73. doi:10.1073/pnas.1511003112
2. Buscarinu MC, Cerasoli B, Annibali V, *et al*. Altered intestinal permeability in patients with relapsing-remitting multiple sclerosis: A pilot study. *Mult Scler*. Mar 2017;23(3):442-446. doi:10.1177/1352458516652498
3. Lakes EH, Allen KD. Gait analysis methods for rodent models of arthritic disorders: reviews and recommendations. *Osteoarthritis Cartilage*. Nov 2016;24(11):1837-1849. doi:10.1016/j.joca.2016.03.008
4. MacKenzie SJ, Yi JL, Singla A, Russell TM, Calancie B. Innervation and function of rat tail muscles for modeling cauda equina injury and repair. *Muscle Nerve*. Jul 2015;52(1):94-102. doi:10.1002/mus.24498
5. Davies AL, Desai RA, Bloomfield PS, *et al*. Neurological deficits caused by tissue hypoxia in neuroinflammatory disease. *Ann Neurol*. 12/2013 2013;74(6):815-825. doi:10.1002/ana.24006 [doi]
6. Desai R. A study of mitochondrial biogenesis in the rodent nervous system. Ph.D. Thesis. University College London; 2015.
7. Campbell GR, Mahad DJ. A Method to Detect Cytochrome c Oxidase Activity and Mitochondrial Proteins in Oligodendrocytes. *Methods Mol Biol*. 2019;1936:333-342. doi:10.1007/978-1-4939-9072-6_19
8. Levenson RM, Mansfield JR. Multispectral imaging in biology and medicine: slices of life. *Cytometry A*. Aug 1 2006;69(8):748-58. doi:10.1002/cyto.a.20319
9. Amatruda M, Harris K, Matis A, *et al*. Oxygen treatment reduces neurological deficits and demyelination in two animal models of multiple sclerosis. *Neuropathol Appl Neurobiol*. Dec 15 2023;49:e12868. doi:10.1111/nan.12868
10. Desai RA, Davies AL, Tachrount M, *et al*. Cause and prevention of demyelination in a model multiple sclerosis lesion. *Ann Neurol*. 1/27/2016 2016;79:591-604. doi:10.1002/ana.24607 [doi]
11. Sadeghian M, Mastrolia V, Haddad AR, *et al*. Mitochondrial dysfunction is an important cause of neurological deficits in an inflammatory model of multiple sclerosis. *Scientific Reports*. 2016 2016;6:33249.
12. Desai RA, Davies AL, Del Rossi N, *et al*. Nimodipine reduces dysfunction and demyelination in models of multiple sclerosis. *Ann Neurol*. Jul 2020;88(1):123-136. doi:10.1002/ana.25749
13. Parihar A, Vaccaro P, Ghafourifar P. Nitric oxide irreversibly inhibits cytochrome oxidase at low oxygen concentrations: evidence for inverse oxygen concentration-dependent peroxynitrite formation. *Iubmb Life*. 1/2008 2008;60(1):64-67. doi:10.1002/iub.12 [doi]
14. Calcerrada P, Peluffo G, Radi R. Nitric oxide-derived oxidants with a focus on peroxynitrite: molecular targets, cellular responses and therapeutic implications. *Curr Pharm Des*. Dec 2011;17(35):3905-32. doi:10.2174/138161211798357719
15. Monti L, Morbidelli L, Bazzani L, Rossi A. Influence of Circulating Endothelin-1 and Asymmetric Dimethylarginine on Whole Brain Circulation Time in Multiple Sclerosis. *Biomark Insights*. 2017;12:1177271917712514. doi:10.1177/1177271917712514
16. Aboul-Enein F, Lassmann H. Mitochondrial damage and histotoxic hypoxia: a pathway of tissue injury in inflammatory brain disease? *Acta Neuropathol (Berl)*. 1/2005 2005;109(1):49-55.
17. Mascali D, Villani A, Chiarelli AM, *et al*. Pathophysiology of multiple sclerosis damage and repair: Linking cerebral hypoperfusion to the development of irreversible tissue loss in multiple sclerosis using magnetic resonance imaging. *Eur J Neurol*. Aug 2023;30(8):2348-2356. doi:10.1111/ene.15827

18. Owens TS, Calverley TA, Stacey BS, *et al*. Contact events in rugby union and the link to reduced cognition: evidence for impaired redox-regulation of cerebrovascular function. *Exp Physiol*. Sep 2021;106(9):1971-1980. doi:10.1113/EP089330
19. Bailey DM, Jones DW, Sinnott A, *et al*. Impaired cerebral haemodynamic function associated with chronic traumatic brain injury in professional boxers. *Clin Sci (Lond)*. Feb 2013;124(3):177-89. doi:10.1042/CS20120259
20. Salehi A, Zhang JH, Obenaus A. Response of the cerebral vasculature following traumatic brain injury. *J Cereb Blood Flow Metab*. Jul 2017;37(7):2320-2339. doi:10.1177/0271678X17701460
21. Sweeney MD, Kisler K, Montagne A, Toga AW, Zlokovic BV. The role of brain vasculature in neurodegenerative disorders. *Nat Neurosci*. Oct 2018;21(10):1318-1331. doi:10.1038/s41593-018-0234-x

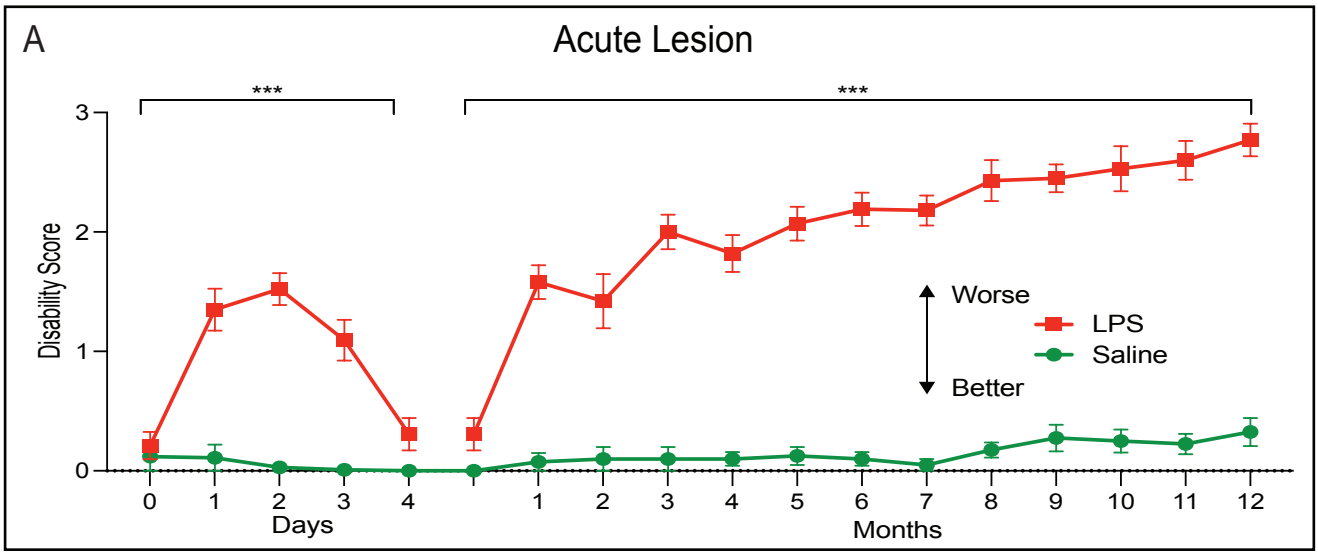
A
Acute Lesion
***
***
Disability Score
Days
Months
Worse
Better
LPS
Saline

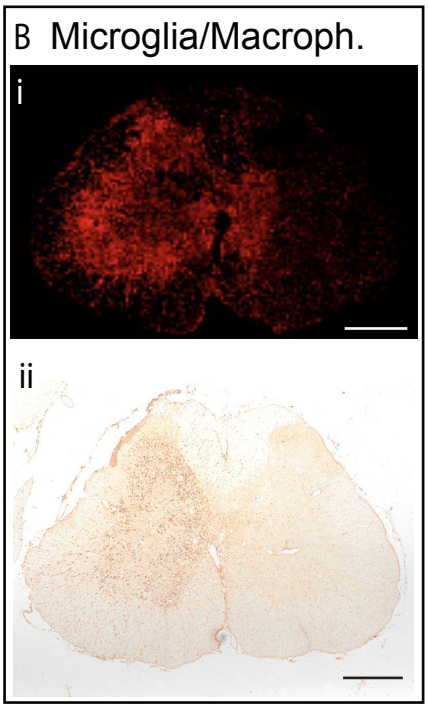
B Microglia/Macroph.
i
ii

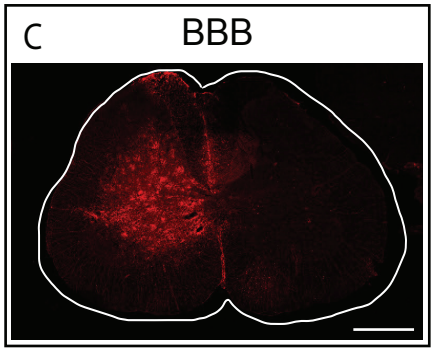
C
BBB

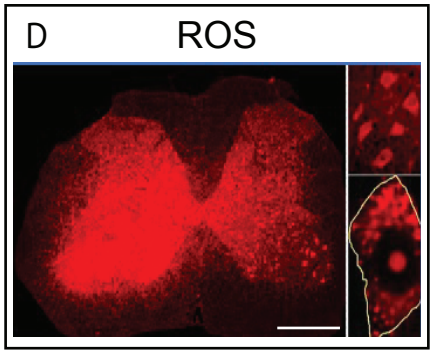
D
ROS

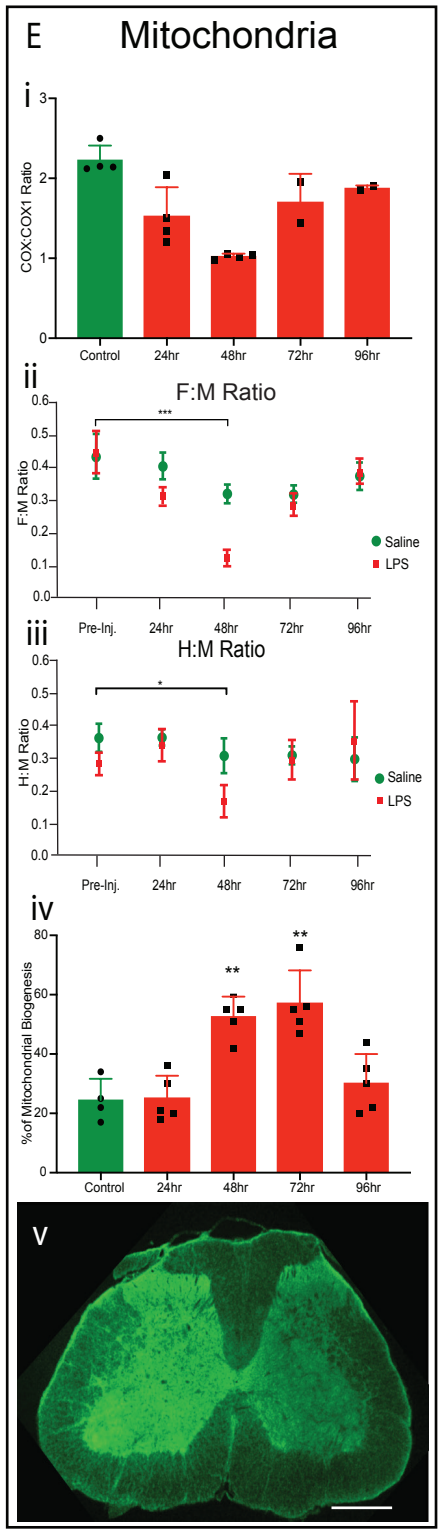
E
Mitochondria
i
COX:COX1 Ratio
Control
24hr
48hr
72hr
96hr
ii
F:M Ratio
F:M Ratio
Saline
LPS
iii
H:M Ratio
H:M Ratio
iv
%of Mitochondrial Biogenesis
v

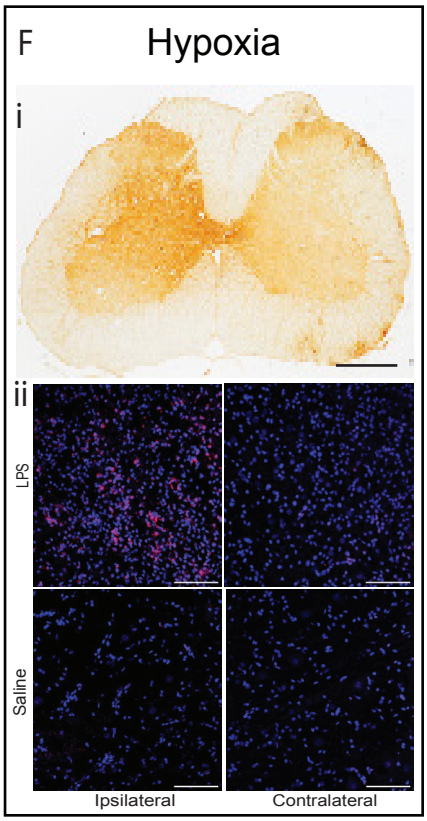
F
Hypoxia
i
ii
LPS
Saline
Ipsilateral
Contralateral

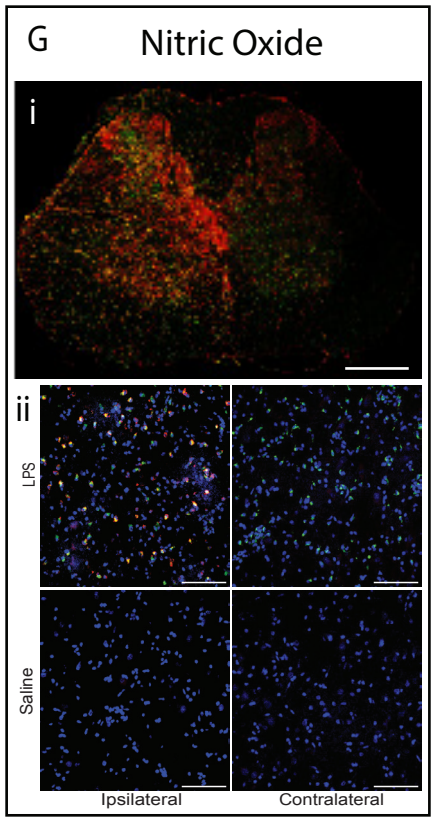
G
Nitric Oxide
i
ii
LPS
Saline
Ipsilateral
Contralateral

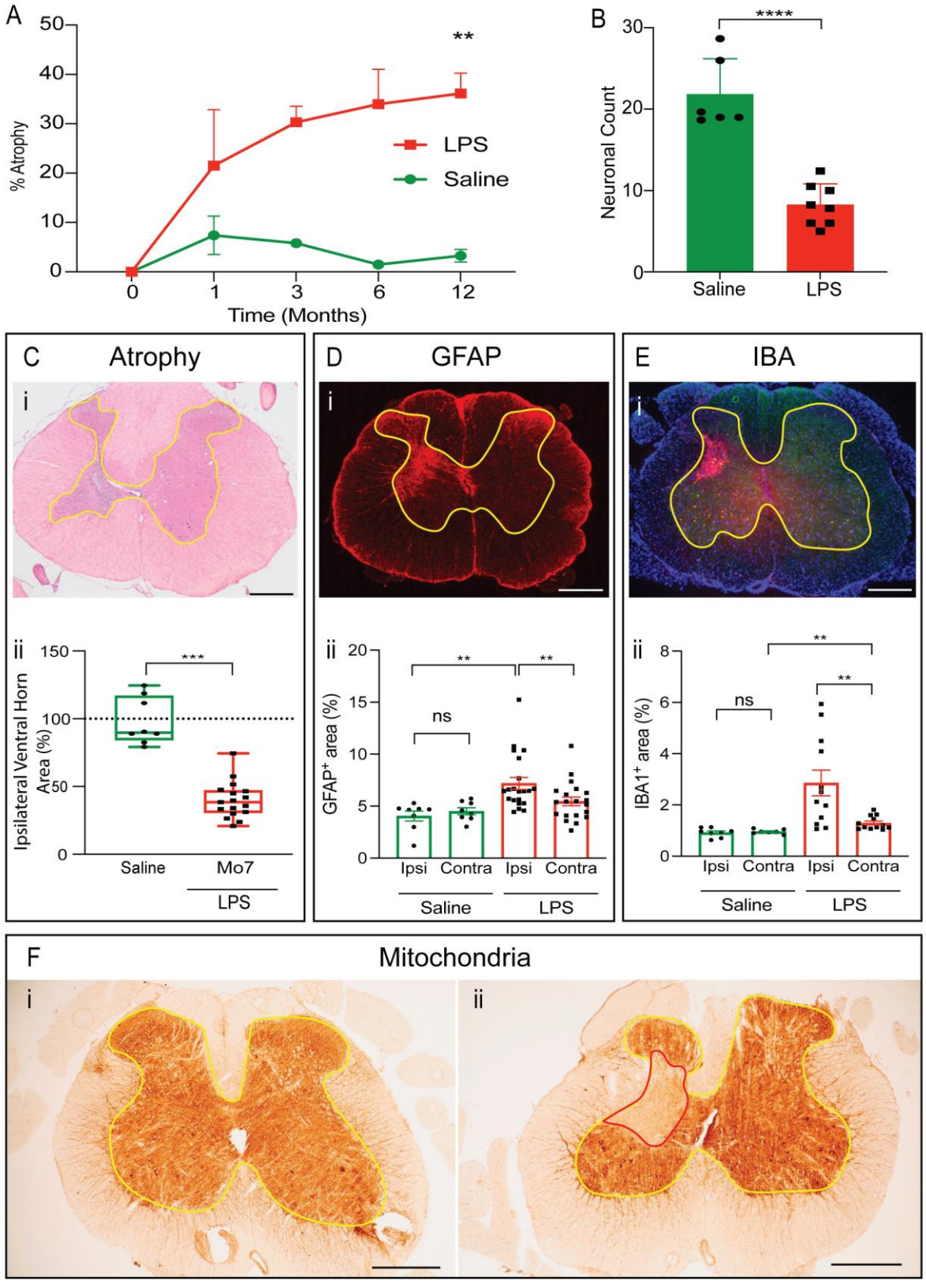
A
% Atrophy
50
40
30
20
10
0
**
LPS
Saline
0
1
3
6
12
Time (Months)
B
Neuronal Count
30
20
10
0
****
Saline
LPS
C
Atrophy
i
ii
Ipsilateral Ventral Horn Area (%)
150
100
50
0
***
Saline
Mo7
LPS
D
GFAP
i
ii
GFAP+ area (%)
20
15
10
5
0
**
**
ns
Ipsi
Contra
Ipsi
Contra
Saline
LPS
E
IBA
i
ii
IBA1+ area (%)
8
6
4
2
0
**
**
ns
Ipsi
Contra
Ipsi
Contra
Saline
LPS
F
Mitochondria
i
ii

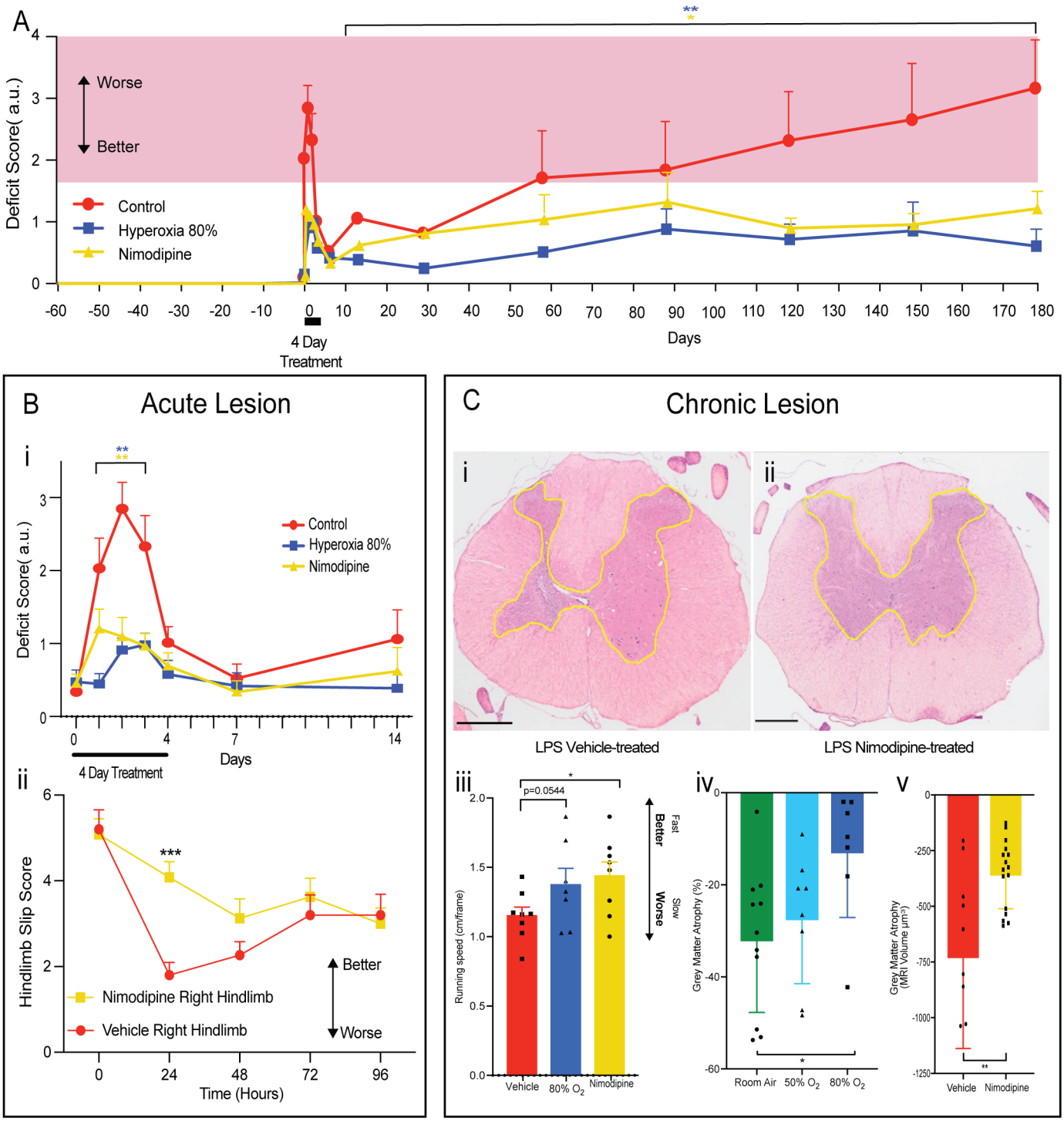
A
Deficit Score(a.u.)
Worse
Better
Control
Hyperoxia 80%
Nimodipine
4 Day Treatment
Days
B
Acute Lesion
i
Deficit Score(a.u.)
Control
Hyperoxia 80%
Nimodipine
4 Day Treatment
Days
ii
Hindlimb Slip Score
Nimodipine Right Hindlimb
Vehicle Right Hindlimb
Better
Worse
Time (Hours)
C
Chronic Lesion
i
ii
LPS Vehicle-treated
LPS Nimodipine-treated
iii
p=0.0544
Running speed (cm/frame)
Fast
Better
Slow
Worse
Vehicle
80% O2
Nimodipine
iv
Grey Matter Atrophy (%)
Room Air
50% O2
80% O2
v
Grey Matter Atrophy (MRI Volume µm3)
Vehicle
Nimodipine

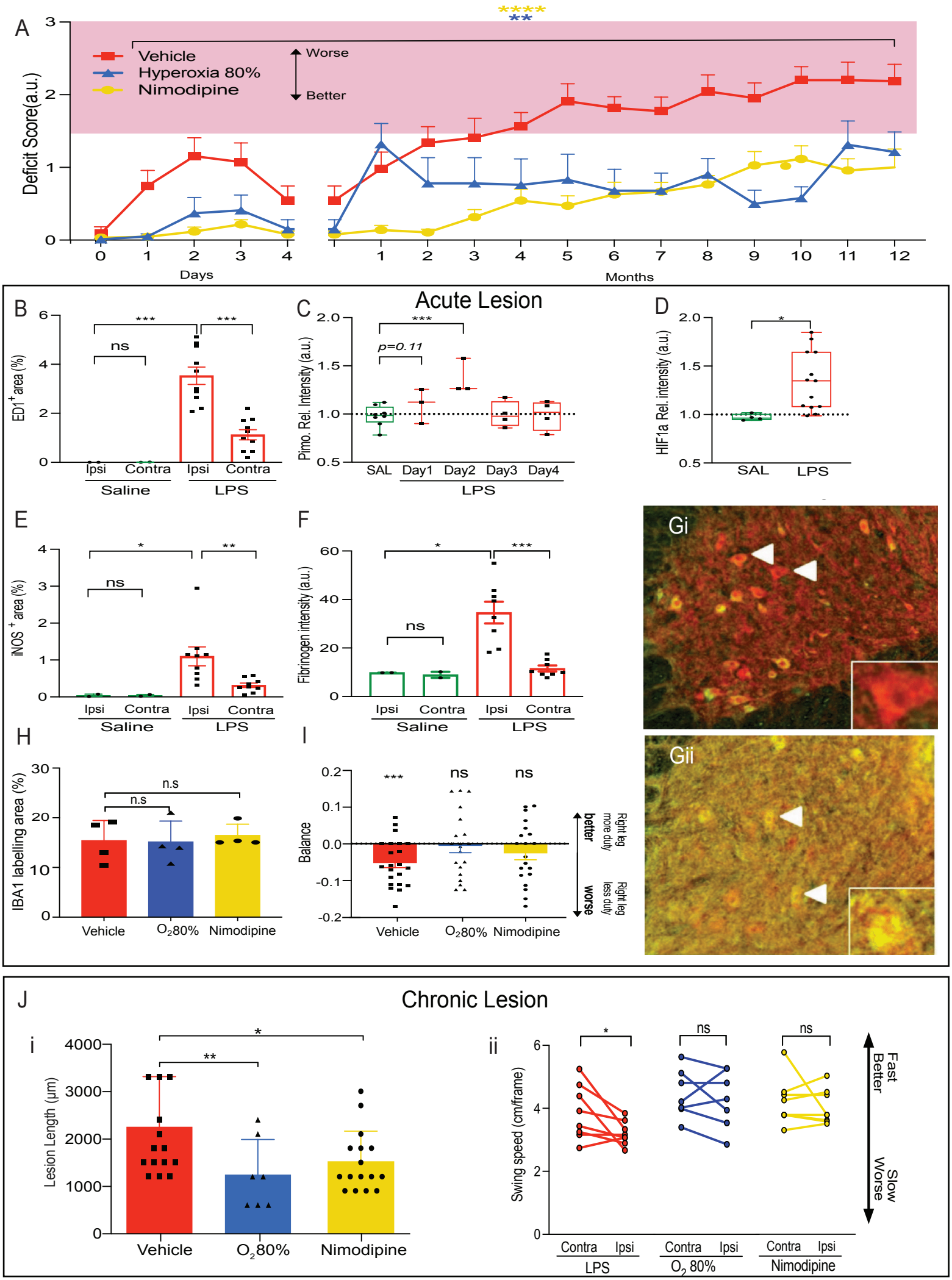
A
Vehicle
Hyperoxia 80%
Nimodipine
Worse
Better
Deficit Score(a.u.)
Days
Months
****
**
Acute Lesion
B
ED1+ area (%)
ns
***
***
Ipsi
Contra
Ipsi
Contra
Saline
LPS
C
Pimo. Rel. Intensity (a.u.)
p=0.11
SAL
Day1
Day2
Day3
Day4
LPS
D
HIF1a Rel. intensity (a.u.)
SAL
LPS
E
iNOS+ area (%)
F
Fibrinogen intensity (a.u.)
Gi
Gii
H
IBA1 labelling area (%)
n.s
Vehicle
O2 80%
Nimodipine
I
Balance
better
worse
Right leg more duty
Right leg less duty
J
Chronic Lesion
i
Lesion Length (µm)
ii
Swing speed (cm/frame)
Fast
Better
Slow
Worse
LPS
O2 80%
Nimodipine